Composition dependence of the infrared dielectric functions in Si-doped hexagonal $Al_xGa_{1-x}N$ films on *c*-plane sapphire substrates

Z. G. Hu,[1] M. Strassburg,[1,2] N. Dietz,[1] A. G. U. Perera,[1,*] A. Asghar,[2] and I. T. Ferguson[2,3]
[1]*Department of Physics and Astronomy, Georgia State University, Atlanta, Georgia 30303, USA*
[2]*School of Electrical and Computer Engineering, Georgia Institute of Technology, Atlanta, Georgia 30332, USA*
[3]*School of Materials Science and Engineering, Georgia Institute of Technology, Atlanta, Georgia 30332, USA*
(Received 16 February 2005; revised manuscript received 30 September 2005; published 21 December 2005)

The optical properties of hexagonal $Al_xGa_{1-x}N$ (x from 0.05 to 0.42) epitaxial films with Si doping concentrations up to 10^{18} cm^{-3} grown on *c*-plane sapphire substrates by metal-organic chemical vapor deposition have been investigated using infrared reflectance spectra. The dielectric functions ($\varepsilon=\varepsilon_1+i\varepsilon_2$) of the $Al_xGa_{1-x}N$ films are determined in the wavelength region of 1.54–50 μm at room temperature. The experimental reflectance spectra are analyzed using classical harmonic Lorentz oscillators and Drude model in the transparent, reststrahlen, and free carrier absorption regions. GaN-like E_1 transverse-optical (TO) phonon frequency linearly decreases and its strength increases with decreasing Al composition. However, AlN-like E_1(TO) phonon frequency shows a relatively weak composition dependence and its strength increases with increasing composition. At a wavelength of 1.54 μm, ε_1 varies between 4.86 and 5.2 when the composition x changes from 0.05 to 0.42 and ε_2 is close to zero. The longitudinal-optical phonon plasmon (LPP) coupled modes of *n*-type hexagonal $Al_xGa_{1-x}N$ films are also discussed. For samples with higher concentrations beyond 10^{18} cm^{-3} the upper LPP coupled mode frequencies increase with increasing carrier concentration indicating the transition from phononlike to plasmonlike behavior.

DOI: 10.1103/PhysRevB.72.245326 PACS number(s): 78.20.Ci, 78.30.Fs, 78.66.Fd, 81.70.Fy

I. INTRODUCTION

Progress in the design and development of group-III nitride optoelectronic devices depends on a better understanding of the optical properties of hexagonal AlN and GaN semiconductors, and their alloys.[1–3] The interest in these alloys stems from the possibility of varying the different electrical and optical properties over a wide spectral range by controlling the alloy composition.[4] The infrared (IR) optical response of these alloys is important not only for optoelectronic device designs, but also for the determination of crystalline quality and free carrier concentrations. These values can be characterized from phonon modes and plasma frequencies, respectively.[5] GaN and $Al_xGa_{1-x}N$ films can be deposited on sapphire (α-Al_2O_3), silicon (Si), silicon carbide (SiC), or GaAs substrates by many different growth techniques.[1,4,6] They crystallize in a thermodynamically stable hexagonal wurtzite structure (α phase) and exhibit a uniaxial optical anisotropy except for layers grown on GaAs substrate, for which films with metastable cubic (β phase) structure were reported.[6,7] For hexagonal $Al_xGa_{1-x}N$ films with space group C_{6v}^4, the A_1 and E_1 optical phonons have transverse-optical (TO) and longitudinal-optical (LO) branches, which are both IR and Raman active according to the selection rules.[3] The optical and/or vibrational properties of the $Al_xGa_{1-x}N$ films have been studied theoretically (random element isodisplacement) and experimentally (IR spectra and Raman scattering).[8–12] However, most studies focused on one- or two-mode behavior of optical phonons in the reststrahlen regions and the impact of stress due to the crystalline mismatch between film and substrate. Note that IR or Raman experimental data (position and broadening) of AlN-like E_1(TO) phonon mode are sparse compared to the $Al_xGa_{1-x}N$ films with low compositions. This may be due to the mixing effects of the E_1 and E_2 optical phonons, in particular for layers on sapphire substrates.[4,10] While Schubert *et al.* reported results on the AlN-like E_1 phonon mode using IR spectroscopic ellipsometry, the Al composition is still limited (x=0.17, 0.28 and 0.5).[13,14] Here, we report seven different Al fractions in the same range. Recently, Kasic *et al.* reported on the optical properties of hexagonal GaN and cubic $Al_xGa_{1-x}N$ films ($x\leqslant 0.20$) using IR spectroscopic ellipsometry.[2,6] Wisniewski *et al.* investigated the E_1(TO) phonon mode of the $Al_xGa_{1-x}N$ films on SiC substrates using IR reflectance spectra.[11] The composition intervals are large and IR optical constants were not given.[11] Yu *et al.* reported the IR optical functions of undoped $Al_xGa_{1-x}N$ films on GaN sapphire substrates in the wavelength region of 1.54–22 μm (i.e., 450–6500 cm^{-1}).[15] Although there are reports on the dielectric functions of the $Al_xGa_{1-x}N$ films in ultraviolet (UV) and visible (Vis) ranges,[16] the IR dielectric properties of $Al_xGa_{1-x}N$ epilayers with different Al compositions and carrier concentrations are still not completely known. The optical constants play an important role in the optoelectronic device designs. Our interest is the analysis of the IR dielectric functions of $Al_xGa_{1-x}N$ films with different compositions, corresponding to smaller spacings in Al content.

IR reflectance spectroscopy is a nonintrusive probe technique, which is an attractive and powerful tool for optical characterizations of the $Al_xGa_{1-x}N$ film materials. Compared to Raman scattering, it not only determines phonon mode characteristics, but also provides the dielectric function of the layers. For IR response and/or lattice vibrations of semiconductor materials, the harmonic Lorentz oscillator model is the most common expression, which can be successfully applied in one-or multimode behavior for semiconductors.[17]

On the other hand, a factorized model, which takes the independent broadening value for each TO and LO phonon mode into account, has recently been used to model IR reflectance spectra and polarized spectra (such as spectroscopic ellipsometry) of GaN and $Al_xGa_{1-x}N$ films.[2,15] According to the known generalized Lowndes condition,[2,18] the factorized model can be transformed into the harmonic Lorentz oscillator model if the broadening value of each TO and LO phonon mode is equal, respectively. Therefore, the harmonic Lorentz oscillator model should be valid as well for the $Al_xGa_{1-x}N$ films, which normally have a two-mode behavior for the A_1(TO) and E_1(TO) phonons (i.e., GaN-like and AlN-like, respectively). Moreover, Holtz *et al.* and Wisniewski *et al.* showed that the harmonic Lorentz oscillator model can be used to calculate IR reflectance spectra of the films under near-normal and oblique angle of incident configurations.[3,11]

The LO phonon plasmon (LPP) coupling is one of the important phenomena in doped semiconductor materials. The experimental studies of LPP coupled modes of the GaN films with different carrier concentrations have been reported previously.[2,19] The LPP coupled modes permit the determination of carrier concentration from IR reflectance spectra or Raman scattering if the effective mass and high-frequency dielectric constants are known. It was found that the presence of free carriers in GaN films can result in a high-frequency shift of LO phonons due to the formation of the LPP coupling.[4] Moreover, the LPP coupled modes become complex for hexagonal $Al_xGa_{1-x}N$ films with different carrier concentrations due to alloying effects. To our knowledge, the LPP coupled modes of hexagonal $Al_xGa_{1-x}N$ films with different compositions and carrier concentrations grown on sapphire substrate have not been studied so far.

In this article, the IR optical properties of $Al_xGa_{1-x}N$ ($0.05 \leqslant x \leqslant 0.42$) epitaxial films with carrier concentration up to 10^{18} cm^{-3} deposited on sapphire substrates are investigated using near-normal incident reflectance spectra. A theoretical model is presented to fit the experimental reflectance spectra. The effects of the Al composition and carrier concentration on GaN-like and AlN-like E_1(TO) phonons, IR dielectric functions, and LPP coupled modes will be discussed in detail.

II. EXPERIMENTAL DETAILS

A. Film growth

Hexagonal $Al_xGa_{1-x}N$ expitaxial films in a wide composition range from 0.05 to 0.42 were grown on *c*-plane sapphire substrates by metal-organic chemical vapor deposition (MOCVD). The layers were deposited using a modified Veeco Discovery series D-125 GaN MOCVD reactor with a vertical injection system. Trimethylgallium (TMGa) and trimethylaluminum (TMAl) were used as group III precursors and ammonia (NH_3) as group V precursor, respectively. The $Al_xGa_{1-x}N$ films were Si doped using silane (SiH_4) diluted in hydrogen as the dopant source. All expitaxial films exhibit *n*-type conductivity. The $Al_xGa_{1-x}N$ layers were grown on top of thin AlN buffer layers (about 20 nm) on a sapphire substrate. This approach improves the crystalline quality of the expitaxial films that were also studied by high-resolution x-ray diffraction (HRXRD) and room temperature UV transmittance spectroscopy. Three different sets of the film samples were grown. The growth was performed at 1050 °C at a reactor pressure of 100 mbars. A V/III ratio of ~2000 was used. The first set has different Al compositions (less than 20%), which were deposited by varying the molar flow of Al into the growth reactor. In the second set of samples, the Al and Ga molar flows were changed in order to obtain the Al compositions between 20% and 30%. For higher compositions (exceeding 30%) the growth temperature was increased up to ~1200 °C. The composition of the epilayer is determined by the HRXRD and the UV transmittance spectroscopy. $\omega-2\theta$ scans were performed revealing the full width at half maximum (FWHM) of the (002) peak for the $Al_xGa_{1-x}N$ epilayers ranging from 320 arcsec to 395 arcsec, which confirms the high crystalline quality. An increase in FWHM was detected with increasing Al concentration. According to Vegard's law, the Al concentration was determined as listed in Table I and was confirmed by the UV transmittance spectroscopy that was applied to determine the position of the optical band gap (see Fig. 1). A steep absorption edge was observed in the samples, and the band gap of the $Al_xGa_{1-x}N$ film was defined by the onset of the absorption. A monotonous increase of the optical band gap was observed with increasing Al concentration. Compared to the HRXRD results, a good agreement was achieved assuming a bowing parameter of $b=0.3$ eV for the optical band gap (E_{gap}) dependence

$$E_{gap}(x) = E_{gap}^{GaN} + (E_{gap}^{AlN} - E_{gap}^{GaN} + b)x + bx^2, \qquad (1)$$

as summarized by Lee *et al.*[20] and as also shown in the inset of Fig. 1. Deviation from more recent publications of the bowing parameter may be attributed to the band-tail states due to composition fluctuations, to the broadening of the excitonic absorption at room temperature, and to the increasing free exciton binding energy, all contributing to the deviation of the optical band-gap energy and hence of the bowing parameter.[21] Nevertheless, it was found in good agreement

TABLE I. Al composition x, carrier concentration n_e from Hall-effect measurements and nominal thickness of the $Al_xGa_{1-x}N$ films on sapphire substrates. Best-fit values of thickness and the 90% confidence limits are given in parentheses. The signal n.a. indicates the data are not available.

		Thickness (nm)		
Sample	x HRXRD	IR	Nominal	n_e ($\times 10^{17}$ cm^{-3})
1084an	0.42	441 (2)	500	1.1
1095an	0.38	348 (1)	650	0.32
1096an	0.32	460 (2)	920	n.a.
1113an	0.26	430 (1)	540	54.6
1115an	0.21	498 (2)	700	73.6
1100an	0.14	562 (1)	550	29
1102an	0.05	1210 (2)	1290	n.a.

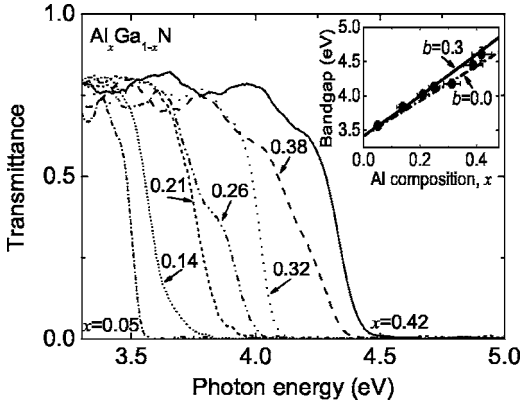

FIG. 1. Transmittance spectra of the $Al_xGa_{1-x}N$ epilayers with variation in the Al composition recorded at room temperature. The inset shows the detected onset edge in the transmittance as a function of the Al composition as determined by the HRXRD measurements. The line data suggest a bowing parameter b between 0 and 0.3 eV.

with the HRXRD results. The film thickness was measured using a real-time reflectance probe technique.[22] The nominal thicknesses of the $Al_xGa_{1-x}N$ epilayers are between 500 and 1300 nm. The carrier concentrations of the layers ranging from 10^{17} to 10^{18} cm^{-3} were analyzed by Hall-effect measurements. The properties of the epilayers are also summarized in Table I.

B. Infrared spectral measurement

Mid-IR (MIR) and far-IR (FIR) reflectance spectra were measured at room temperature over the wavelength range of 1.54–50 μm (i.e., 200–6500 cm^{-1}) using a nitrogen purged Perkin-Elmer system 2000 Fourier transform infrared (FTIR) spectrometer. The reflectance measurements were recorded at near-normal incident configuration (the angle of incidence is 8°) by spectral reflectance accessory (Graseby Specac Ltd.). For the MIR region of 450–6500 cm^{-1} (1.54–22 μm), a liquid nitrogen cooled MCT detector and optimized KBr beamsplitter were used with a resolution of 4 cm^{-1}. A TGS/POLY detector and a 6 μm-thick mylar beamsplitter were employed for the measurements in the FIR region of 200–700 cm^{-1} (14.3–50 μm) with a resolution of 2 cm^{-1}. Gold (Au) and aluminum (Al) mirrors, whose absolute reflectances were directly measured, were used as references for the reflectance spectra in the MIR and FIR regions, respectively. The reflectance spectra in the overlapped regions (about 450–500 cm^{-1}) are in good agreement within the experimental uncertainty of 5%. Due to the small incident angle and the use of unpolarized incident light, the optical anisotropy of hexagonal $Al_xGa_{1-x}N$ films could not be resolved.[3] The reflectance spectrum of one-side-polished sapphire substrate was measured in order to derive its IR dielectric function.

III. RESULTS AND DISCUSSION

A. Theoretical model

Since the reststrahlen regions of sapphire overlap with those of $Al_xGa_{1-x}N$, it is difficult to assign the phonon frequencies directly from the measured reflectance spectra. A model interpretation is necessary to extract the phonon modes and the dielectric function of the layer. The presence of an AlN buffer layer between the $Al_xGa_{1-x}N$ films and the sapphire substrate can be neglected in our analysis since its thickness is approximately 20 nm and the induced error is smaller than 1%.[23] Thus a three-phase model (air/film/substrate) is used to calculate the reflectance spectra of the $Al_xGa_{1-x}N$ films. The reflectance of the single layer on the substrate is calculated by Snell's law and/or Maxwell's equations assuming the layer to be isotropic.[22,24] The optical component of each layer is expressed by a 2×2 matrix. The matrix method is used to calculate the IR reflectance since it enables easy calculation of the reflectance for an arbitrary number of parallel and isotropic layers. Suppose the dielectric function of the film is ε, vacuum is unity, and the substrate is ε_s, respectively. The resultant matrix C_r is described by the following product form:

$$C_r = C_{vf} C_f C_{fs}. \tag{2}$$

Here, the interface matrix between vacuum and film has the form

$$C_{vf} = \frac{1}{2\sqrt{\varepsilon}} \begin{bmatrix} (\sqrt{\varepsilon}+1) & (\sqrt{\varepsilon}-1) \\ (\sqrt{\varepsilon}-1) & (\sqrt{\varepsilon}+1) \end{bmatrix}, \tag{3}$$

and the propagation matrix for the film with thickness d is described by the equation

$$C_f = \begin{bmatrix} \exp(i2\pi\sqrt{\varepsilon}d/\lambda) & 0 \\ 0 & \exp(-i2\pi\sqrt{\varepsilon}d/\lambda) \end{bmatrix}, \tag{4}$$

where λ is the incident wavelength, and correspondingly the interface matrix between film and substrate is

$$C_{fs} = \frac{1}{2\sqrt{\varepsilon_s}} \begin{bmatrix} (\sqrt{\varepsilon_s}+\sqrt{\varepsilon}) & (\sqrt{\varepsilon_s}-\sqrt{\varepsilon}) \\ (\sqrt{\varepsilon_s}-\sqrt{\varepsilon}) & (\sqrt{\varepsilon_s}+\sqrt{\varepsilon}) \end{bmatrix}, \tag{5}$$

thus, the reflectance R can be readily obtained from

$$R = \left| \frac{C_{r1,0}}{C_{r1,1}} \right|^2. \tag{6}$$

The multireflections from substrate are not considered in Eq. (6) because the sapphire substrate is one-side polished. Moreover, there are strong phonon absorptions in the reststrahlen regions of the sapphire.

For polar semiconductor materials, IR dielectric response can be described by the harmonic Lorentz oscillator model, in which the dielectric function is defined as a response function having many pairs of simple poles.[25] Although the A_1 and E_1 optical phonons are both IR active for hexagonal $Al_xGa_{1-x}N$ films, near-normal incident reflectance spectra using unpolarized incident light can only probe the E_1 phonon. The reflectance spectra are only sensitive to the perpendicular tensor compared with p-polarized spectra.[3,11] Two Lorentz oscillators can be considered for GaN-like and AlN-like phonon responses, respectively. The contribution from free carrier to the dielectric function for doped semiconductors is commonly written in the classical Drude model, which is the simplest form because n-type materials have only one free

carrier species (i.e., free electron). Therefore, IR dielectric function of the $Al_xGa_{1-x}N$ films can be written as

$$\varepsilon = \varepsilon_\infty + \sum_{j=1}^{2} \frac{S_j \omega_{TO,j}^2}{\omega_{TO,j}^2 - \omega^2 - i\omega\Gamma_j} - \frac{\varepsilon_\infty \omega_p^2}{\omega^2 + i\omega\gamma}. \quad (7)$$

Here, ε_∞, $\omega_{TO,j}$, S_j, Γ_j, ω_p, and γ represent, in order, the high-frequency dielectric constants, GaN-like and AlN-like E_1(TO) phonon frequencies, the oscillator strengths, the broadening values of E_1(TO) phonons, the plasma frequencies, and the phenomenological damping constants. The plasma frequency of free carriers with effective mass m^* and carrier concentration n_e are given by the following equation:

$$\omega_p = \sqrt{\frac{n_e q^2}{\varepsilon_o \varepsilon_\infty m^*}}, \quad (8)$$

where q is the magnitude of the electron charge and ε_o is the vacuum permittivity.

The best-fit parameter values in Eq. (7) can be found using a Levenberg-Marquardt algorithm, which is an efficient nonlinear calculation method for many parameter fitting.[26] The fitting is based on minimizing the following error function χ:

$$\chi^2 = \frac{1}{N}\sum_{i=1}^{N} |R_{i,exp} - R_{i,cal}|^2, \quad (9)$$

where N is the number of experimental data points, and $R_{i,exp}$ and $R_{i,cal}$ are the experimental and calculated values, respectively. The dielectric function of the substrate should be required in order to model the reflectance spectra of the $Al_xGa_{1-x}N$/sapphire multilayer structures. The reflectance spectrum of sapphire has also been recorded and is used to derive the dielectric function using the fitting procedure. In the present work, the IR dielectric function of *c*-plane sapphire is nearly identical to the reported values.[15,18]

B. FTIR reflectance spectra

Knowledge of the dielectric function for sapphire substrate (shown in Fig. 2) is a prerequisite for analyzing the $Al_xGa_{1-x}N$ epitaxial films in order to identify the influences from the substrate. Note that the real part of the dielectric function is almost constant and the imaginary part is zero below a wavelength of 10 μm, indicating that the sapphire substrate is transparent in this region. Four phonon modes in the wavelength region of 10–30 μm were observed and assigned to 26.1 μm (383 ± 0.4 cm^{-1}), 22.9 μm (436 ± 0.4 cm^{-1}), 17.6 μm (567 ± 0.5 cm^{-1}), and 15.8 μm (633 ± 0.3 cm^{-1}), respectively. The high-frequency dielectric constant is 3.12 ± 0.01, located between 3.07 (Ref. 18) and 3.2.[27] The above fitted results are similar to the vibration modes perpendicular to the *c* axis. However, the dielectric function near peak wavelengths in the present work is slightly lower than those in Ref. 18. This may be due to the optical anisotropic effect of sapphire, which is uniaxial positive in the wavelength regions close to the reststrahlen bands, and the reflectance loss since it is one-side polished. Different substrate wafers also can result in small deviations of the dielectric function. The IR dielectric function for the substrate is used in all subsequent model calculations for the $Al_xGa_{1-x}N$ films.

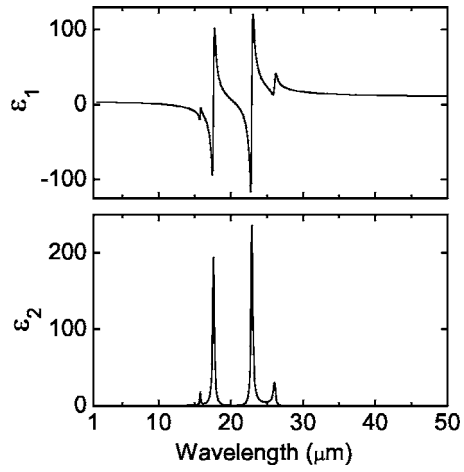

FIG. 2. Infrared dielectric function for the sapphire substrate is derived from the reflectance spectrum.

The experimental reflectance spectra of the $Al_xGa_{1-x}N$ epitaxial films with the composition x from 0.05 to 0.42 are shown in Fig. 3 (dotted lines). The wavelength unit (μm) is used for clarity on the effects from free carriers. The broadening edge at 11 μm (910 cm^{-1}) is ascribed to the reststrahlen band of the sapphire, which is close to the LO frequency of 909 cm^{-1} (the corresponding TO frequency is 633 cm^{-1}). In the long wavelength regions, two peaks located at about 22.9 μm and 26.1 μm are from the sapphire and peak intensities decrease with increasing film thickness. Note that the first peak (22.9 μm) disappears for the $Al_{0.05}Ga_{0.95}N$ film, whose thickness is two times greater than other values and almost to 1.2 μm.

Although the phonons of sapphire substrate dominate the measured reflectance spectra, the phonon characteristics of the $Al_xGa_{1-x}N$ films are still visible. The reflectance spectra

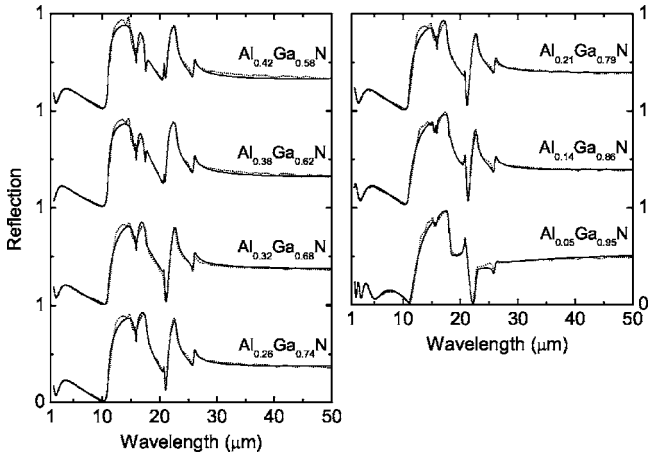

FIG. 3. Experimental infrared reflectance spectra (dotted lines) of the $Al_xGa_{1-x}N$ films on sapphire with different compositions, thicknesses and carrier concentrations and their best fit results (solid lines). For clarity, each spectrum is successively shifted by 1 in the vertical direction.

TABLE II. Lorentz oscillator and Drude parameter values in Eq. (7) are from the best fit to the infrared reflectance spectra of the $Al_xGa_{1-x}N$ films in Fig. 3. The 90% confidence limits of the fitting parameters are given in parentheses. The strength S is dimensionless, and all other parameters are in cm^{-1}. For clarity, the Al compositions are listed in the table again.

		GaN-like mode			AlN-like mode			Free carriers	
Sample	x	S	ω_{TO}	Γ	S	ω_{TO}	Γ	ω_p	γ
1084an	0.42	3.21	584	18.6	1.1	643	28.8	364	50
		(0.08)	(0.8)	(1.4)	(0.08)	(0.9)	(2.1)	(13.3)	(12.5)
1095an	0.38	3.25	583	24.8	1.05	644	31.2	343	114
		(0.08)	(0.7)	(1.5)	(0.07)	(0.8)	(2.1)	(16.4)	(18)
1096an	0.32	3.48	574	(15.1)	0.83	641	35.7	596	543
		(0.08)	(1)	(1.7)	(0.08)	(1.4)	(3.5)	(12)	(22.6)
1113an	0.26	3.61	568	7.4	0.47	638	33.4	497	270
		(0.06)	(0.8)	(1.2)	(0.05)	(1.5)	(3.9)	(8.4)	(11.4)
1115an	0.21	3.68	570	7.1	0.52	638	31.8	558	368
		(0.07)	(0.9)	(1.5)	(0.06)	(1.6)	(4.2)	(9.5)	(14.3)
1100an	0.14	3.85	560	3.8	0.1	648	18.3	513	353
		(0.04)	(0.6)	(1)	(0.02)	(1.4)	(3.8)	(5)	(8.4)
1102an	0.05	3.61	560	2.3	0.05	640	17.1	592	380
		(0.04)	(0.5)	(0.8)	(0.01)	(2.2)	(6.1)	(4.5)	(8.1)

have some differences with increasing composition in the reststrahlen regions as shown in Fig. 3. For the $Al_xGa_{1-x}N$ films with $x=0.38$ and 0.42, the peak around 17.1 μm (585 cm^{-1}) is weaker than the other values and shifts towards longer wavelength (lower energy). This peak is the strongest for the $Al_{0.05}Ga_{0.95}N$ film with the approximate position of 17.8 μm (561 cm^{-1}). It is due to GaN-like phonon effects since the position is close to the known GaN E_1(TO) phonon frequency.[1,3] The high compositions can result in the phonon line broadening and asymmetry.[4,10] The reflectance spectra of the $Al_xGa_{1-x}N$ films with $x=0.32$, 0.26, 0.21 and 0.14 have similar spectral shapes. There is a dip at 15.8 μm (632 cm^{-1}) for the reflectance spectra of all films. The dip intensity increases and its position slightly shifts towards high frequency with increasing Al composition. Similar results were reported by Yu *et al.*[15] and the value was about 645 cm^{-1} for undoped $Al_xGa_{1-x}N$ films. There it was considered to be related to the E_2 phonon mode. The observed differences may be due to free carrier effects since all studied epitaxial films are doped. The carrier concentration effect can be clearly seen in longer wavelength region (beyond 25 μm). With increasing carrier concentration the reflectance spectral intensity shows an increasing trend. For $Al_xGa_{1-x}N$ films (with successive compositions and small intervals) grown on sapphire substrate, there are no detailed reports on IR reflectance spectra.

C. Phonon modes

For deriving IR dielectric function and phonon frequencies, the model calculation used is based on the previous discussions (Sec. III A). The calculated reflectance spectra using Eq. (6) are shown in Fig. 3 (solid lines). A good agreement between the calculated and experimental data is obtained in the entire wavelength region. The model calculations have a standard deviation $\chi \leqslant 1.5\times10^{-2}$ for all spectra. In the reststrahlen regions the fitting quality is also good. The small differences are assigned to the effects of a thin AlN buffer layer, which has been neglected in the calculation model. It should be noted that the high-frequency constants ε_∞ of the $Al_xGa_{1-x}N$ films varying from 4.94 ± 0.02 to 5.26 ± 0.02, are located between the values 4.84 for AlN and 5.35 for GaN.[3] They are slightly higher than the values of 4.2 to 5.01 reported in Ref. 15. The differences may be explained by a wider fitting range and/or due to free carrier effects in the present work. Also the effect of free carriers on the high-energy transitions can directly affect the high-frequency dielectric constants, which is considered in the harmonic Lorentz oscillator model. The best-fit parameters in Eq. (7) and fitting errors are listed in Tables I and II. The fitting errors of the Lorentz oscillator parameters are much smaller than those of the Drude parameters, which generally have strong parameter correlations. From Table I, the calculated thicknesses are closer to the nominal values for the $Al_xGa_{1-x}N$ films with $x=0.42$, 0.26, 0.14, and 0.05. However, there is a larger deviation for the other three samples (0.38, 0.32, and 0.21).

It can be concluded that the strength of GaN-like E_1(TO) phonon increases with decreasing composition except for the $Al_{0.05}Ga_{0.95}N$ film, whose value (3.61) is slightly less [see Fig. 4(a) and Table II]. The strength of AlN-like E_1(TO) phonon shows an opposite trend. Note that the differences between oscillator strengths are proportional to the deviations of the Al composition for the $Al_xGa_{1-x}N$ films. Moreover, our results (composition dependence and value magnitudes) for the oscillator strengths are closer to the theoretical calculation data for the E_1 phonon mode.[28] Wisniewski *et al.* reported that the oscillator strength of E_1(TO) phonon shows

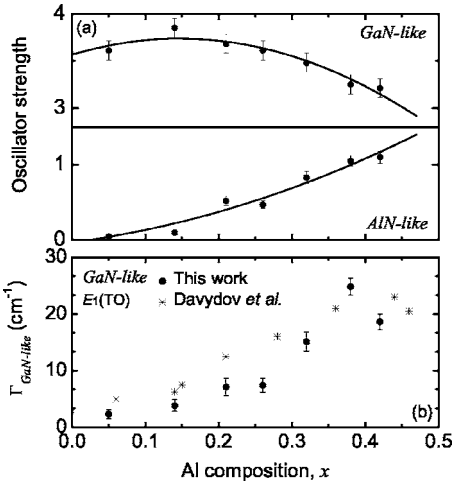

FIG. 4. (a) Composition dependence of the oscillator strength of GaN-like and AlN-like E_1(TO) phonons for the $Al_xGa_{1-x}N$ films. Polynomial fits (solid lines) are applied to emphasize the nonlinearity and guide the eyes. (b) Composition dependence of the broadening value of GaN-like E_1(TO) phonon. All data points except for the stars in (b), which are from Raman scattering in Ref. 4, are listed in Table II.

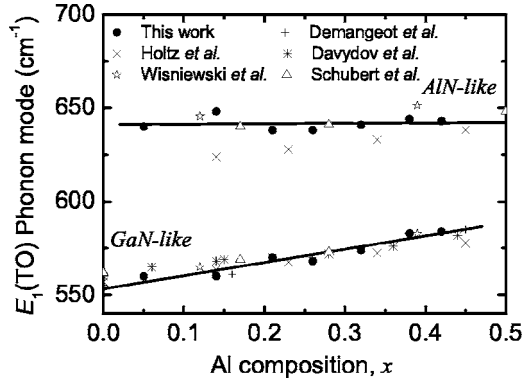

FIG. 5. Composition dependence of GaN-like and AlN-like E_1(TO) phonon frequencies for the $Al_xGa_{1-x}N$ films, determined by the infrared reflectance spectra. Solid lines represent the linear curve fitting results in this work. Note that the films from different references were deposited on different substrates. The detailed discussions can be found in Sec. III C.

a linear dependence on the composition for the $Al_xGa_{1-x}N$ films on SiC substrates.[11] However, the present results indicate that the composition dependence of the oscillator strength deviates from the linear behavior as shown in Fig. 4(a). It is reported that the substrate materials can affect the phonon mode characteristics of the films. The present epitaxial films are deposited on sapphire substrates, which results in the discrepancy compared to SiC substrates.[29] The number of samples used in Ref. 11 is small and the interval in compositions is very large (more than 25%). For the present work, a much larger set of epitaxial film samples, which have a smaller Al composition interval (about 6%), was employed to obtain the information. The oscillator strength mechanism for the $Al_xGa_{1-x}N$ films on different substrate materials need to be further investigated.

GaN-like E_1(TO) phonon frequency decreases with decreasing Al composition and AlN-like E_1(TO) phonon frequency shows relatively weak composition dependence as shown in Fig. 5. There, the results from Refs. 3, 4, 10, 11, and 13 are added for a comparison. It should be emphasized that the film samples in the literature were deposited on different substrates and either their carrier concentrations were not mentioned or were lower than our values. The present work gives a linear dependence of the mode energy on the Al composition range from 0.05 to 0.42: $(553+71x)$ cm^{-1} for GaN-like E_1(TO) phonon frequency and $(641+2x)$ cm^{-1} for AlN-like E_1(TO) phonon frequency. The values for GaN-like E_1(TO) phonon frequency are similar to the following results: $(557+46x)$ cm^{-1} (Ref. 3) and $(557+66x)$ cm^{-1} (Ref. 11), which are from the full composition range. Moreover, the present linear relation of GaN-like E_1(TO) phonon frequency is suitable for all experimental data from the literature in Fig. 5. Also this linear relation can provide a better approximation on GaN-like E_1(TO) phonon frequency for the $Al_xGa_{1-x}N$ films. However, the present values for AlN-like E_1(TO) phonon frequency $(641+2x)$ cm^{-1} are nearly between two sets of data: $(617+47x)$ cm^{-1} (Ref. 3) and $(643+21x)$ cm^{-1} (Ref. 11) AlN-like E_1(TO) phonon frequency has weak linear dependence on the composition in the present work. It is reasonable because the $Al_xGa_{1-x}N$ films have relatively low Al compositions, which mainly occupy near a GaN branch. The carrier concentrations and different lattice mismatches can result in shifting the phonon frequency. This indicates that the substrate can affect AlN-like E_1(TO) phonon mode.

The broadening values of GaN-like E_1(TO) phonons show an increasing trend (from 2.3 to 24.8 cm^{-1}) with the composition, which is much smaller than the values reported (about from 20 to 35 cm^{-1}).[3,11] It indicates that the epitaxial films have good crystalline quality. As shown in Fig. 4(b), our results confirm the increase in the broadening value of GaN-like E_1(TO) phonons, approximately from 3 to 23cm^{-1}, with increasing composition (for the $Al_xGa_{1-x}N$ films on sapphire substrates grown using molecular beam epitaxy) as suggested by Davydov *et al.*[4] Obviously, the broadening values of GaN-like E_1(TO) phonons for the $Al_xGa_{1-x}N$ films on sapphire substrates are smaller than those for the films on Si and SiC substrates. The broadening values of AlN-like E_1(TO) phonons varied between 17.1 and 35.7 cm^{-1}, which is significantly less than the values of AlN E_1(TO) phonons in Refs. 11 and 13. Note that no other reports on the subject could be found for hexagonal $Al_xGa_{1-x}N$ epitaxial films on sapphire substrates. Therefore, the present work also provides important information on the broadening values of AlN-like E_1(TO) phonons studied with IR reflectance spectra.

The Drude fitting parameters in Eq. (7) suggest that the plasma frequency ω_p and damping constants γ increase with increasing carrier concentration, which strongly indicate that the electron scattering times decrease in the epitaxial films. Generally, the carrier concentration can be calculated using the fitted values with Eq. (8), if the effective mass is known. Similarly, the effective mass can be calculated if the carrier concentration is obtained from Hall-effect measurements. As

shown in Fig. 3, the matches between the calculated and experimental spectra improve with increasing carrier concentration. The electron effective mass ($m^*=0.22m_0$, here m_0 is the free electron mass) for *n*-type GaN was used to approximately calculate the carrier concentration, resulting in values of about $(3-5)\times10^{18}$ cm^{-3}. These values agree with Hall-effect measurements except for the two highest Al compositions. The Hall-effect measurement may have a larger error for higher compositions due to the strong decrease in the carrier concentration and the increase in resistivity. The plasma frequency obtained from the FIR measurement usually depends on the experimental wavelength limit.[30] Therefore, FIR measurement should extend to longer wavelengths (i.e., plasma frequency edges) for the film samples with lower carrier concentrations. The wavelength limit of 50 μm (i.e., 200 cm^{-1}) is suitable for most of our samples with a concentration on the order of 10^{18} cm^{-3} in the present work. Due to lower carrier concentrations and the measured wavelength limit is out of the plasma frequency (less than 200 cm^{-1} for lower carrier concentrations), stronger parameter correlations exist between the plasma frequency and damping constants in the numerical fitting regression analysis for the $Al_{0.42}Ga_{0.58}N$ and $Al_{0.38}Ga_{0.62}N$ films, whose fitting errors are larger than the others (Table II). These may explain the discrepancies between the electrical and optical measurements. Nevertheless, their fitted plasma frequencies are definitely less than those of other samples, which approximately confirms the variation trend of the carrier concentrations from the Hall-effect measurements (Table I). Note that the dependence of the effective mass on the composition is not considered in the calculations, which may result in larger deviations for the epilayers with higher compositions. In addition, the $Al_xGa_{1-x}N$ epitaxial films were deposited on 2-inch sapphire substrate. The diffusion of Si dopant and uniformity of the epitaxial films may be difficult to be controlled in the growth processing. Moreover, the measured sample volumes and the electric contacts in Hall-effect measurements also can induce the above differences between the electrical and optical results, which are from the contactless and noninvasive probe experiments with very small volumes (the light spot is about 4 mm in diameter).[31]

D. Dielectric functions

The determination of the dielectric functions for film materials generally depends on several methods, including transmittance spectra, reflectance spectra, and spectroscopic ellipsometry. The transmittance spectra is only valid when the substrate is transparent in the studied wavelength regions.[16] However, the reflectance spectra and spectroscopic ellipsometry are very useful tools for the opaque substrates.[6,13–15] Note that the reflectance spectra may be more simple than spectroscopic ellipsometry, which is commercially inaccessible (in particular for the far-infrared region). In addition, the dielectric functions are the basic parameters for far-infrared detector designs. The total absorption of detectors based on doped $Al_xGa_{1-x}N$ materials can be calculated using the obtained dielectric functions. From the above analysis, all fitted parameter values are reasonable and can be used to derive the dielectric functions. The real part ε_1 and imaginary part ε_2 of IR dielectric functions of the $Al_xGa_{1-x}N$ films with different compositions are shown in Figs. 6(a) and 6(b). The dielectric function of the $Al_{0.42}Ga_{0.38}N$ film is plotted in the entire wavelength region as an example given the similar shape for all epilayers. In the transparent region (1.54–10 μm), the real part slightly decreases with increasing wavelength. At the wavelength of 1.54 μm, the real part is between 4.86 and 5.2 (refractive index is correspondingly about 2.21 and 2.28) according to different compositions. This is closer to the reported values (2.2–2.3) obtained from the transmission spectra in the UV and Vis region at the wavelength of 0.85 μm. Note that there are no strong dispersion contributions in the discontinued regions.[16] The imaginary part is zero, indicating the epitaxial films are transparent. As shown in Fig. 6, the dielectric function shows a two-peak structure in the reststrahlen region (10–25 μm), which is due to the two-mode behavior of the E_1(TO) phonon. The strong peak at about 17.1 μm (585 cm^{-1}) can be ascribed to the contributions from GaN-like E_1(TO) phonons. This peak value for ε_1 varies from 47 to 441.1 and for ε_2 change from 78 to 836.9 with decreasing Al composition. However, the other peak at about 15.6 μm (641 cm^{-1}) is weak and assigned to the contribution from AlN-like E_1(TO) phonons. The variation of this weak peak with Al composition is shown in the inset in Fig. 6. For the $Al_{0.05}Ga_{0.95}N$ film, this peak nearly disappears and the dielectric function is close to the values of the pure GaN materials. In the long wavelength, the free carrier behavior plays an important role in the optical response. Beyond a wavelength of 25 μm, the imaginary part of the dielectric function quickly increases with increasing wavelength due to the free carrier absorption for all epitaxial films. Despite some discrepancies in the compositions, the results indicate

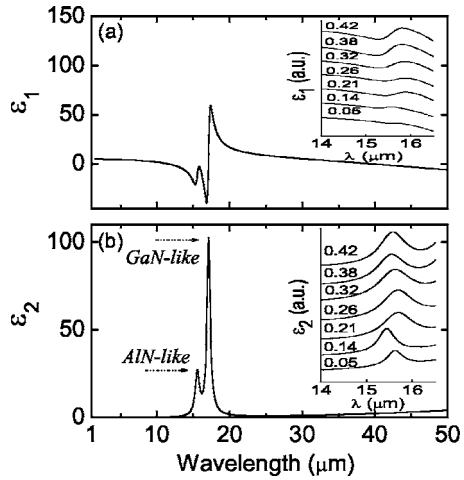

FIG. 6. Evolution of the dielectric functions (a) ε_1 and (b) ε_2 for the $Al_xGa_{1-x}N$ films with different compositions on sapphire substrates. For example, the dielectric function of the $Al_{0.42}Ga_{0.58}N$ film in the transparent, reststrahlen, and free carrier absorption regions is shown. The inset shows the peak from AlN-like E_1(TO) phonons, the wavelength scale is limited from 14 to 16.5μm. The arrows indicate the peaks from AlN-like and GaN-like E_1(TO) phonon modes.

that high carrier concentration results in higher dielectric function in the wavelength region of 25–50 μm.

The absorption coefficient of n-type $Al_{0.14}Ga_{0.86}N$ with a carrier concentration of 2.9×10^{18} cm^{-3} is about 6.5×10^{3} cm^{-1} at a wavelength of 50 μm. This value is slightly higher than the results of the $Al_xGa_{1-x}As$ films in the long wavelength region.[32] The values reported here for the IR dielectric function of the $Al_xGa_{1-x}N$ epitaxial films ($0.05 \leqslant x \leqslant 0.42$) on sapphire substrates with successive compositions support novel optoelectronic devices, such as AlGaN/GaN UV-Vis and IR dual band detectors.[33]

E. LPP coupled modes

The nature of the LPP coupled modes in ternary alloy systems is very complex as a consequence of the two-mode behavior of their zone-center optical modes.[34,35] The situation becomes more striking for the $Al_xGa_{1-x}N$ materials due to the overlapped region between E_1(LO) (about 750 cm^{-1} for GaN) and AlN-like E_1(TO) phonon frequencies (about 640 cm^{-1}). Some literature reported that there is a one-mode behavior of E_1(LO) mode in $Al_xGa_{1-x}N$ based on the experimental data.[4,10] However, Wisniewski *et al.* argued that it is due to unresolved low-frequency branch of E_1(LO) phonons, which is at least an order of magnitude weaker than the high-frequency branch.[11] Different intensity of low- and high-frequency branches of the E_1(LO) phonon, as claimed by Wisniewski *et al.*,[11] may explain the experimental observation of one-mode behavior in previous literature.[4,10] Moreover, the LPP coupled mode strongly depends on the damping constants of free carrier. A larger damping constant results in a broadening and suppresses the peak intensity of the low-frequency branch. Unfortunately, the values of the low-frequency branch and fitted damping constants were not given and discussed in the above work.

Generally, there are three modes which are labeled as LPP$^-$, L^0, and LPP$^+$ for the ternary alloy systems. If the carrier concentration is not high, the LPP$^-$ mode changes from low plasma frequency to GaN-like TO phonon frequency. Correspondingly, the LPP$^+$ mode shifts from AlN-like TO to LO phonon frequency. The LPP$^+$ mode becomes plasmonlike when plasmon frequency is beyond the LO phonon frequency. On the other hand, the L^0 mode should be close to AlN-like TO phonon frequency (Note that AlN-like phonon is overlapped by GaN-like phonon.) Figure 7 shows the spectral density function Im$(-1/\varepsilon)$ of the $Al_xGa_{1-x}N$ films with different compositions and carrier concentrations. Not only do the strength and position of the LPP coupled modes depend on the composition, but also on the carrier concentration since free carriers result in a high-frequency shift of LO phonon frequency. Two main peaks located at 300 cm^{-1} and 850 cm^{-1} are determined and assigned to the low-frequency branch LPP$^-$ and high-frequency branch LPP$^+$. In Table III these values are listed as a function of the composition and carrier concentration. For relatively low Al compositions ($x \leqslant 0.21$), the LPP$^-$ mode increases with increasing carrier concentration. However, the competition between the effects from the composition and carrier concentration appears. The broadening value for the LPP$^-$ mode of

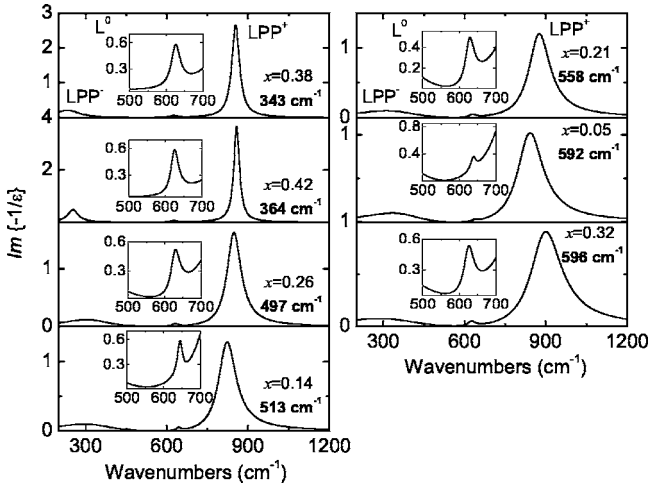

FIG. 7. The spectral density function Im$(-1/\varepsilon)$ of the $Al_xGa_{1-x}N$ films with different compositions and carrier concentrations. The inset shows a narrow region of 500–700 cm^{-1} with a factor of 10 enlargement. Note that the carrier concentration (i.e., plasma frequency) and not the Al composition is used as the major parameter to organize the figure.

the $Al_{0.42}Ga_{58}N$ film is the lowest due to the smallest damping constant (Table II). As stated previously, the small peak structure about 630 cm^{-1} in Fig. 7 can be assigned as the L^0 mode although the order of magnitude of the mode is much smaller than the LPP$^-$ and LPP$^+$ branches. It should be emphasized that the low-frequency branches of E_1(LO) phonon reported by Wisniewski *et al.* are close to the L^0 modes in our work [because the measured wavelength only extended to 25 μm (400 cm^{-1}) and the LPP$^-$ branch was not detected in Ref. 11]. The LPP$^+$ mode values are close to E_1(LO) phonon frequency (850 cm^{-1}) for the films with $x=0.38$ and 0.42 due to the lower carrier concentrations. However, for the $Al_xGa_{1-x}N$ films with smaller Al compositions the upper LPP$^+$ modes increase with increasing carrier concentration and show a changing trend from phononlike to plasmonlike behavior for the films with four highest concentrations, whose damping constants are larger. This indicates the ability to derive the LPP coupled modes from the IR reflectance spectra although it is an indirect method. Also it is necessary

TABLE III. LPP coupled mode values of the $Al_xGa_{1-x}N$ films are from the spectral density function Im$(-1/\varepsilon)$ in Fig. 7. All parameters are in cm^{-1}. For clarity, the Al compositions x and fitted plasma frequencies ω_p are listed in the table again.

			LPP mode		
Sample	x	ω_p	LPP$^-$	L^0	LPP$^+$
1084an	0.42	364	254	625	858
1095an	0.38	343	233	626	854
1096an	0.32	596	284	626	901
1113an	0.26	497	304	630	848
1115an	0.21	558	311	629	876
1100an	0.14	513	295	644	823
1102an	0.05	592	334	639	842

to extend the measured wavelength into the far-infrared region in order to clarify the LPP^- and L^0 coupled modes.

IV. CONCLUSIONS

The optical properties of hexagonal $Al_xGa_{1-x}N$ ($0.05 \leqslant x \leqslant 0.42$) films deposited on sapphire substrates have been investigated in the wavelength region of 1.54–50 μm using the reflectance spectroscopy. The dielectric functions in the FIR region were determined by modeling the experimental reflectance spectra for the epitaxial films. The results show that GaN-like E_1(TO) phonon frequency decreases with decreasing Al composition. The linear dependence on the composition of the $Al_xGa_{1-x}N$ films can be found for GaN-like E_1(TO) phonon frequency. AlN-like E_1(TO) phonon frequency shows relatively weak composition dependence. Composition dependent oscillator strengths and broadening values of GaN-like and AlN-like E_1(TO) phonons have been discussed. The dielectric function shows a two-mode behavior in the reststrahlen region. The LPP^-, L^0, and LPP^+ modes for $Al_xGa_{1-x}N$ epitaxial films were observed. It indicates that the L^0 modes have intensities being one order of magnitude less compared to the LPP^+ modes. The LPP^+ modes increase with increasing carrier concentration and show the changing trend from phononlike to plasmonlike behavior.

ACKNOWLEDGMENTS

The work was supported in part by the U.S. NSF under Grant No. ECS-0140434. M. Strassburg acknowledges support from the Alexander von Humboldt-Foundation. The authors would like to acknowledge S. G. Matsik, M. B. M. Rinzan, G. Ariyawansa, and J. Senawiratne for FTIR and transmittance spectroscopy measurements. The authors also wish to acknowledge M. H. Kane and H. Kang for experimental support conducting Hall-effect and HRXRD measurements.

*Electronic address: uperera@gsu.edu

[1] H. Siegle, G. Kaczmarczyk, L. Filippidis, A. P. Litvinchuk, A. Hoffmann, and C. Thomsen, Phys. Rev. B **55**, 7000 (1997).
[2] A. Kasic, M. Schubert, S. Einfeldt, D. Hommel, and T. E. Tiwald, Phys. Rev. B **62**, 7365 (2000).
[3] M. Holtz, T. Prokofyeva, M. Seon, K. Copeland, J. Vanbuskirk, S. Williams, S. A. Nikishin, V. Tretyakov, and H. Temkin, J. Appl. Phys. **89**, 7977 (2001).
[4] V. Yu. Davydov, I. N. Goncharuk, A. N. Smirnov, A. E. Nikolaev, W. V. Lundin, A. S. Usikov, A. A. Klochikhin, J. Aderhold, J. Graul, O. Semchinova, and H. Harima, Phys. Rev. B **65**, 125203 (2002).
[5] P. Y. Yu and M. Cardona, *Fundamentals of Semiconductors* (Springer, Berlin, 1996).
[6] A. Kasic, M. Schubert, T. Frey, U. Köhler, D. J. As, and C. M. Herzinger, Phys. Rev. B **65**, 184302 (2002).
[7] D. J. As, D. Schikora, A. Greiner, M. Lübbers, J. Mimkes, and K. Lischka, Phys. Rev. B **54**, R11118 (1996).
[8] H. Siegle, L. Eckey, A. Hoffmann, C. Thomsen, B. K. Meyer, D. Schikora, M. Hankeln, and K. Lischka, Solid State Commun. **96**, 943 (1995).
[9] H. Grille, Ch. Schnittler, and F. Bechstedt, Phys. Rev. B **61**, 6091 (2000).
[10] F. Demangeot, J. Groenen, J. Frandon, M. A. Renucci, O. Briot, S. Clur, and R. L. Aulombard, Appl. Phys. Lett. **72**, 2674 (1998).
[11] P. Wisniewski, W. Knap, J. P. Malzac, J. Camassel, M. D. Bremser, R. F. Davis, and T. Suski, Appl. Phys. Lett. **73**, 1760 (1998).
[12] T. Kazawa, T. Kachi, H. Kano, Y. Taga, M. Hashimoto, N. Koide, and K. Manabe, J. Appl. Phys. **75**, 1098 (1994).
[13] M. Schubert, A. Kasic, T. E. Tiwald, J. Off, B. Kuhn, and F. Scholz, MRS Internet J. Nitride Semicond. Res. **4**, 11 (1999).
[14] A. Kasic, M. Schubert, J. Off, B. Kuhn, F. Scholz, S. Einfeldt, T. Böttcher, D. Hommel, D. J. As, U. Köhler, A. Dadgar, A. Krost, Y. Saito, Y. Nanishi, M. R. Correia, S. Pereira, V. Darakchieva, B. Monemar, H. Amano, I. Akasaki, and G. Wagner, Phys. Status Solidi C **0**, 1750 (2003).
[15] G. Yu, H. Ishikawa, M. Umeno, T. Egawa, J. Watanabe, T. Soga, and T. Jimbo, Appl. Phys. Lett. **73**, 1472 (1998).
[16] D. Brunner, H. Angerer, E. Bustarret, F. Freudenberg, R. Dimitrov, O. Ambacher, and M. Stutzmann, J. Appl. Phys. **82**, 5090 (1997).
[17] R. Ferrini, M. Galli, G. Guizzetti, M. Patrini, A. Bosacchi, S. Franchi, and R. Magnanini, Phys. Rev. B **56**, 7549 (1997).
[18] M. Schubert, T. E. Tiwald, and C. M. Herzinger, Phys. Rev. B **61**, 8187 (2000).
[19] B. K. Meyer, A. Hoffmann, and P. Thurian, *Group-III Nitride Semiconductor Compounds*, edited by B. Gil (Clarendon, Oxford, 1998).
[20] S. R. Lee, A. F. Wright, M. H. Crawford, G. A. Peterson, J. Han, and R. M. Biefeld, Appl. Phys. Lett. **74**, 3344 (1999).
[21] J. Wagner, H. Obloh, M. Kunzer, M. Maier, K. Köhler, and B. Johs, J. Appl. Phys. **89**, 2779 (2001).
[22] N. Dietz, Mater. Sci. Eng., B **87**, 1 (2001).
[23] We also tried a four-phase model (air/film/AlN/sapphire) to fit the reflectance spectra, the results are almost the same as that from the three-phase model in the 90% confidence limit. The thickness (20 nm) of the buffer layer is too small compared with the measured wavelength. Hence, the uesd near-normal incident confuguration is not sensitive for thin buffer layers.
[24] O. S. Heaven, *Optical Properties of Thin Solid Films* (Dover, New York, 1991).
[25] J. Humlíček, R. Henn, and M. Cardona, Phys. Rev. B **61**, 14554 (2000).
[26] W. H. Press, S. A. Teukolsky, W. T. Vetterling, and B. P. Flannery, *Numerical Recipes in C: The Art of Scientific Computing* (Cambridge University Press, Cambridge, MA, 1992).
[27] A. S. Barker, Jr., Phys. Rev. **132**, 1474 (1963).
[28] S. G. Yu, K. W. Kim, L. Bergman, M. Dutta, M. A. Stroscio, and J. M. Zavada, Phys. Rev. B **58**, 15283 (1998).
[29] C. Kisielowski, J. Krüger, S. Ruvimov, T. Suski, J. W. Ager III, E. Jones, Z. Liliental-Weber, M. Rubin, E. R. Weber, M. D.

Bremser, and R. F. Davis, Phys. Rev. B **54**, 17745 (1996).
[30] T. E. Tiwald, J. A. Woollam, S. Zollner, J. Christiansen, R. B. Gregory, T. Wetteroth, S. R. Wilson, and A. R. Powell, Phys. Rev. B **60**, 11464 (1999).
[31] Z. G. Hu, M. B. M. Rinzan, S. G. Matsik, A. G. U. Perera, G. Von Winckel, A. Stintz, and S. Krishna, J. Appl. Phys. **97**, 093529 (2005).
[32] M. B. M. Rinzan, D. G. Esaev, A. G. U. Perera, S. G. Matsik, G. Von Winckel, A. Stintz, and S. Krishna, Appl. Phys. Lett. **85**, 5236 (2004).
[33] G. Ariyawansa, M. B. M. Rinzan, D. G. Esaev, S. G. Matsik, G. Hastings, A. G. U. Perera, H. C. Liu, B. N. Zvonkov, and V. I. Gavrilenko, Appl. Phys. Lett. **86**, 143510 (2005).
[34] O. K. Kim and W. G. Spitzer, Phys. Rev. B **20**, 3258 (1979).
[35] J. W. Orton and C. T. Foxon, Rep. Prog. Phys. **61**, 1 (1998).